A thylakoid membrane-bound and redox-active rubredoxin (RBD1) functions in de novo assembly and repair of photosystem II

José G. García-Cerdán[a,b,1,2], Ariel L. Furst[c], Kent L. McDonald[d], Danja Schünemann[e], Matthew B. Francis[c,f], and Krishna K. Niyogi[a,b,g,2]

[a]Howard Hughes Medical Institute, University of California, Berkeley, CA 94720; [b]Department of Plant and Microbial Biology, University of California, Berkeley, CA 94720-3102; [c]Department of Chemistry, University of California, Berkeley, CA 94720-1460; [d]Electron Microscope Laboratory, University of California, Berkeley, CA 94720; [e]Molecular Biology of Plant Organelles, Ruhr-University Bochum, 44780 Bochum, Germany; [f]Materials Sciences Division, Lawrence Berkeley National Laboratory, Berkeley, CA 94720-1460; and [g]Molecular Biophysics and Integrated Bioimaging Division, Lawrence Berkeley National Laboratory, Berkeley, CA 94720

Edited by Donald R. Ort, University of Illinois at Urbana–Champaign, Urbana, IL, and approved June 25, 2019 (received for review February 26, 2019)

Photosystem II (PSII) undergoes frequent photooxidative damage that, if not repaired, impairs photosynthetic activity and growth. How photosynthetic organisms protect vulnerable PSII intermediate complexes during de novo assembly and repair remains poorly understood. Here, we report the genetic and biochemical characterization of chloroplast-located rubredoxin 1 (RBD1), a PSII assembly factor containing a redox-active rubredoxin domain and a single C-terminal transmembrane α-helix (TMH) domain. RBD1 is an integral thylakoid membrane protein that is enriched in stroma lamellae fractions with the rubredoxin domain exposed on the stromal side. RBD1 also interacts with PSII intermediate complexes containing cytochrome b_{559}. Complementation of the *Chlamydomonas reinhardtii* (hereafter *Chlamydomonas*) RBD1-deficient *2pac* mutant with constructs encoding RBD1 protein truncations and site-directed mutations demonstrated that the TMH domain is essential for de novo PSII assembly, whereas the rubredoxin domain is involved in PSII repair. The rubredoxin domain exhibits a redox midpoint potential of +114 mV and is proficient in 1-electron transfers to a surrogate cytochrome *c* in vitro. Reduction of oxidized RBD1 is NADPH dependent and can be mediated by ferredoxin-NADP$^+$ reductase (FNR) in vitro. We propose that RBD1 participates, together with the cytochrome b_{559}, in the protection of PSII intermediate complexes from photooxidative damage during de novo assembly and repair. This role of RBD1 is consistent with its evolutionary conservation among photosynthetic organisms and the fact that it is essential in photosynthetic eukaryotes.

photosynthesis | rubredoxin | photosystem II | *Chlamydomonas*

Photosystem II (PSII) is a multisubunit pigment–protein complex within the thylakoid membranes (TMs) of cyanobacteria, algae, and plants. PSII catalyzes the light-driven oxidation of water and associated reduction of plastoquinone in the first steps of linear electron flow in oxygenic photosynthesis (1, 2). The de novo biogenesis of PSII monomers in both cyanobacteria and chloroplasts occurs stepwise via transient formation of distinct intermediate complexes (3, 4). A key intermediate is the minimal reaction center (RC) complex, formed by assembly of D1 protein into a receptor complex composed of D2, the cytochrome b_{559} (Cyt b_{559}) subunits α (PsbE) and β (PsbF), and PsbI (4). The D1 and D2 proteins of the RC form a heterodimer that binds the majority of the redox-active cofactors required for PSII electron transport, and the RC is capable of carrying out light-induced charge separation but not water splitting (5). Peripherally attached to the RC are the chlorophyll (Chl) *a*-binding core antenna subunits CP47 and CP43. Surrounding these complexes is a set of low–molecular-weight (LMW) subunits of PSII (6). Complete maturation of PSII monomers into water-splitting complexes requires the processing of D1 by the C-terminal peptidase (CtpA) on the luminal side of the TM, ligation of the manganese cluster, and assembly of the oxygen-evolving complex subunits (7, 8).

Before and after acquiring water-splitting activity, PSII complexes are prone to photooxidative damage even under low light conditions (9). This damage leads to reduced photosynthetic linear electron flow that impairs growth (10, 11). In fully assembled PSII complexes, the D1 subunit is the major target of photooxidative damage and undergoes constant degradation and replacement (turnover) in a process known as PSII repair (10–12). The efficiency of photosynthetic electron transfer decreases markedly only when the rate of damage exceeds the rate of repair (13). Associated with PSII intermediate complexes are PSII auxiliary factors that optimize assembly and/or repair following photooxidative damage and are not found in the final, mature PSII complex (14–16). During PSII assembly and repair, intermediate complexes are presumably disconnected from the photosynthetic donor and/or acceptor electron transport chains and are, therefore, without the usual electron sinks and are

Significance

Photosystem II (PSII) catalyzes the light-driven oxidation of water in photosynthesis, supplying energy and oxygen to many life-forms on earth. During PSII assembly and repair, PSII intermediate complexes are prone to photooxidative damage, requiring mechanisms to minimize this damage. Here, we report the functional characterization of RBD1, a PSII assembly factor that interacts with PSII intermediate complexes to ensure their functional assembly and repair. We propose that the redox activity of RBD1 participates together with the cytochrome b_{559} to protect PSII from photooxidation. This work not only improves our understanding of cellular protection mechanisms for the vital PSII complex but also informs genetic engineering strategies for protection of PSII repair to increase agricultural productivity.

Author contributions: J.G.G.-C. and K.K.N. designed research; J.G.G.-C., A.L.F., and K.L.M. performed research; J.G.G.-C., A.L.F., K.L.M., D.S., and M.B.F. contributed new reagents/analytic tools; J.G.G.-C., A.L.F., K.L.M., D.S., M.B.F., and K.K.N. analyzed data; and J.G.G.-C. and K.K.N. wrote the paper.

The authors declare no conflict of interest.

This article is a PNAS Direct Submission.

[1]Present address: Molecular, Cellular and Developmental Biology, University of Colorado Boulder, Boulder, CO 80309.

[2]To whom correspondence may be addressed. Email: jggarcia.cerdan@gmail.com or niyogi@berkeley.edu.

This article contains supporting information online at www.pnas.org/lookup/suppl/doi:10.1073/pnas.1903314116/-/DCSupplemental.

Published online July 29, 2019.

particularly vulnerable to photooxidative damage. This damage can be caused by long-lived Chl $P680^+$, a highly oxidizing molecule formed by charge separation that has a redox potential of +1.2 V (17). When high-energy radical pairs involving Chl recombine, they can form Chl triplet states that react with triplet oxygen to form singlet oxygen, an especially damaging reactive oxygen species (18–20). PSII assembly/repair intermediate complexes require protective mechanisms to minimize this damage and thus facilitate maturation into active PSII complexes.

The mechanism by which PSII intermediate complexes are protected from photooxidative damage remains poorly understood. However, the Cyt b_{559} has been proposed to participate in photoprotection. The Cyt b_{559} is present in all oxygenic photosynthetic organisms, is essential for PSII biogenesis, and binds the only redox-active heme *b* group of PSII. The Cyt b_{559} is not involved in the linear electron transport chain that oxidizes water and reduces plastoquinone (21–23). The protective role is based on the ability of heme *b* to participate in 1-electron transfer from its high-potential form (+390 mV) (24) via β-carotene (CarD2) to reduce the photooxidized primary donor $P680^+$ under donor-side photoinhibitory conditions (e.g., during impairment or assembly of the oxygen-evolving complex) (25, 26). However, a detailed functional description of the Cyt b_{559} redox forms, the cause of their interconversion, and the source of electrons remain unclear (27, 28). In cyanobacteria, the Cyt b_{559} forms part of a well-conserved gene cluster that is key to the biogenesis of PSII (29–31). This gene cluster contains the rubredoxin domain-encoding *rubA* gene, the PSII assembly factor *ycf48*/*HCF136*, and the LMW subunits of PSII formed by the Cyt b_{559} (*psbE* and *psbF*), *psbL*, and *psbJ*. The presence of the rubredoxin in the same gene cluster as the Cyt b_{559} suggests a functional connection between these 2 redox-active proteins during PSII assembly and repair.

Rubredoxins are LMW iron-containing proteins that participate in electron transfer reactions (32, 33). The RubA ortholog in photosynthetic eukaryotes is RBD1 (34). We previously demonstrated that the absence of RBD1 in photosynthetic eukaryotes impacts the functional accumulation of PSII (34). However, the precise role of RBD1 in promoting PSII accumulation remains unknown. To gain insight into the role of RBD1 in PSII assembly and repair and investigate its possible interactions with the Cyt b_{559}, we performed 1) biochemical characterization of PSII assembly in the RBD1-deficient *2pac* mutant of the model green alga *Chlamydomonas* (34), 2) complementation studies of the *2pac* mutant with truncated and site-directed RBD1 mutants, 3) analysis of the biochemical properties of RBD1 in the TM of *Arabidopsis thaliana* (hereafter *Arabidopsis*) and *Chlamydomonas* chloroplasts, and 4) determination of the redox properties of the RBD1 rubredoxin domain. We demonstrate that RBD1 is a stroma lamellae-enriched and redox-active assembly factor that interacts with PSII and ensures functional assembly and repair of PSII complexes in the chloroplast. On the basis of our results, we propose an alternative 1-electron transfer pathway in PSII, powered by NADPH and ferredoxin-$NADP^+$ reductase (FNR), whereby RBD1 acts together with the Cyt b_{559} to protect PSII from photooxidative damage.

Results

RBD1 Promotes Functional Assembly of PSII Monomer Complexes. We previously demonstrated that the absence of RBD1 impacts photosynthetic growth, PSII efficiency, and accumulation of PSII subunits in the *Chlamydomonas 2pac* mutant (Fig. 1*A*) (34). To gain further insight into the PSII assembly process, we studied the organization of TM protein complexes by blue native polyacrylamide gel electrophoresis (BN-PAGE) from heterotrophically grown wild-type (WT) and *2pac* cells (Fig. 1*C*). We found PSII macroorganization to be severely altered in the mutant, with a marked reduction of PSII monomers (PSII-M), dimers (PSII-D), and PSII-LHCII supercomplexes (PSII-SC), while the assembly of photosystem I (PSI) protein complexes and the light-harvesting complexes (LHCs) were normal, in comparison with WT (Fig. 1*C*). To determine to what extent PSII assembly occurs in *2pac* cells, we separated protein complexes from the first dimension (1D) BN-PAGE in a second denaturing dimension (sodium dodecyl sulfate [SDS]/PAGE) and performed immunoblot analyses against RBD1 and the PSII subunits D2 and CP43 (Fig. 1*D*). In WT, the D2 and CP43 immunoblot signals clearly comigrated with PSII-M, PSII-D, and PSII-SC, whereas the RBD1 signals were detected in at least 3 spots. The 2 major spots were in the low mass region of the native gel, containing unassembled and LMW complexes, whereas the third and minor spot comigrated with PSII-M. As expected, the *2pac* mutant exhibited very low levels of D2 and CP43 and no RBD1 (Fig. 1*D*). To obtain D2 and CP43 signals from the mutant, a 1-min film exposure was required, whereas equivalent WT signals were detectable after only a few seconds. The largest PSII complex found in *2pac* membranes contained D2 and CP43 and corresponded to PSII-M, while PSII-D and PSII-SC were undetectable (Fig. 1*D*). These results show that, in the absence of RBD1, the accumulation of PSII-M complexes is severely impaired. We further visualized heterotrophically grown cells by transmission electron microscopy. The *2pac* mutant, in comparison with WT cells, exhibited aberrant chloroplast TM architecture (Fig. 1*B*), which might be related to its relatively high LHCII/PSII ratio.

We next investigated whether RBD1 is present in the chloroplast during light induction of PSII assembly in the *Chlamydomonas* mutant *chlL* (Fig. 1*E*) (35). This mutant is defective in the light-independent protochlorophyllide reductase and is unable to synthesize Chl in the dark; when dark-grown *chlL* cells are exposed to light, pigment accumulation correlates with both TM formation and the synthesis and accumulation of photosynthetic complexes (36, 37). D2 was barely detectable in the dark-grown *chlL* cells and only accumulated after cells were exposed to light (Fig. 1*E*). In contrast, RBD1 was found in high levels in the dark-grown cells and throughout greening (Fig. 1*E*), indicating that RBD1 accumulates before PSII assembly.

RBD1 Is a Membrane-Anchored Protein with the Rubredoxin Domain Exposed to the Stroma. To study how RBD1 associates with the TM, we assayed polypeptide extractions from *Arabidopsis* and spinach TM. Membrane-bound polypeptides were washed with either high ionic chaotropic salts or an alkaline pH (>10) solution (38), followed by centrifugation to separate pelleted membrane fractions (MB) from the extracted soluble fractions (SN) (*SI Appendix*, Fig. S1*B*). The fractions were further subjected to SDS/PAGE and immunoblot analysis with specific anti-RBD1 antibodies. RBD1 was mostly resistant to membrane extraction techniques, although washes with 2 M sodium thiocyanate led to minor extractions of RBD1.

We also studied the topology of the RBD1 rubredoxin domain in the TM by protease protection experiments performed on intact *Arabidopsis* and spinach chloroplasts (Fig. 2*A* and *SI Appendix*, Fig. S1*C*, respectively). As RBD1 is predicted to contain 15 trypsin digestion sites, a protease protection assay was performed by adding trypsin to either hypoosmotically lysed chloroplasts, yielding intact TM, or to samples treated with 0.25% *n*-dodecyl-β-D-maltoside (β-DM) detergent to disrupt TM. When detergent-disrupted membranes were treated with trypsin, both stroma-facing and lumen-enclosed proteins were digested. Photosystem I subunit D (PsaD) was used as a topological marker for stromal orientation (39), and as expected, it was rapidly cleaved to a trypsin-resistant fragment. The disruption of TM by detergent and access to luminal compartment proteins were verified through the digestion of the lumen-localized PsbO subunit of PSII. RBD1, like PsaD, was digested rapidly from

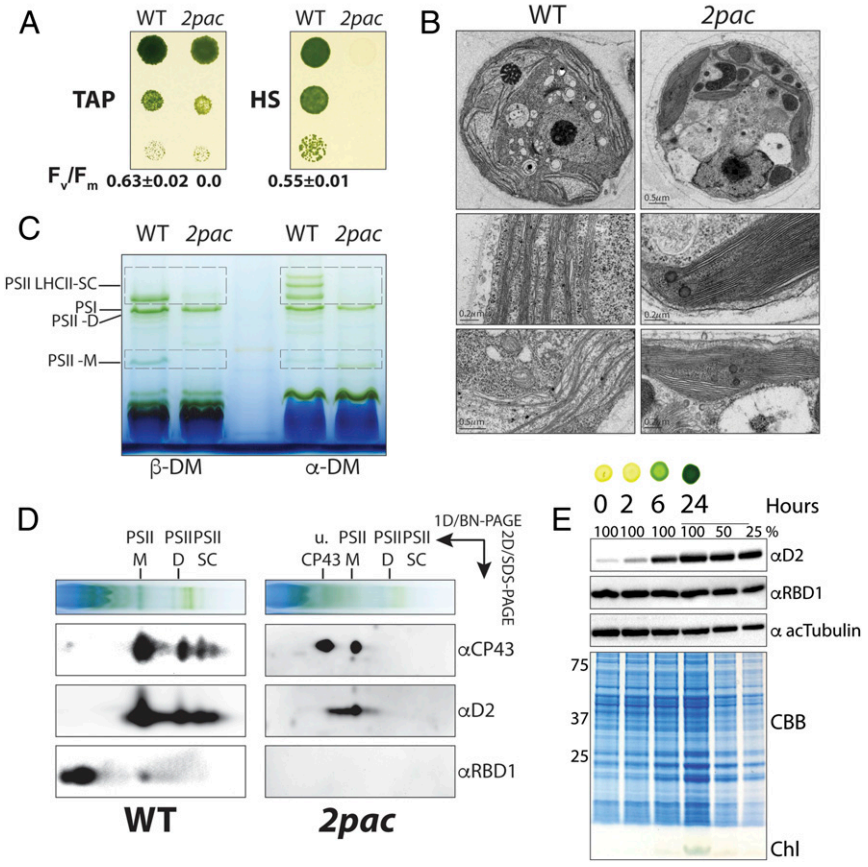

Fig. 1. *2pac* is a nonphotosynthetic mutant with impaired assembly of PSII monomers and abnormal chloroplast architecture. (*A*) Growth phenotype and PSII efficiency (F_v/F_m) of wild-type (WT) and mutant spotted cells grown mixotrophically (TAP) under low light (5 μmol photons·m^{-2}·s^{-1}) or photoautotrophically (HS) under normal light (80 μmol photons·m^{-2}·s^{-1}) conditions. (*B*) Transmission electron microscopy analyses of WT and mutant cells grown heterotrophically. (*C*) BN-PAGE analyses of WT and *2pac* solubilized thylakoid membrane (TM) protein complexes treated with 2 different detergents, α-DM and β-DM. (*D*) The 2D BN/SDS/PAGE and immunoblot analyses from WT and *2pac* solubilized TM protein complexes against PSII subunits D2 and CP43, and RBD1. Immunodetection against D2 and CP43 varies. In WT samples, films were recorded after 5-s exposure compared with 1 min in *2pac* samples. Lanes are labeled as follows: PSI, photosystem I; PSII-D, PSII dimer; PSII-M, PSII monomer; PSII-SC, PSII–LHCII supercomplexes; uCP43, unassembled CP43. (*E*) Immunoblots analyses against D2, RBD1, and acetylated tubulin proteins from greening experiment with the *chlL* mutant, as well as Coomassie-stained SDS/PAGE. Whole-cell samples were collected and subjected to denaturing SDS/PAGE and immunoblot analysis after 0, 6, and 24 h following the shift to normal growth light conditions. One hundred percent loading corresponds to about 1×10^6 cells.

both intact and disrupted TM samples, whereas degradation of PsbO protein occurred only in disrupted membranes (Fig. 2*A* and *SI Appendix*, Fig. S1*C*). These results clearly indicate that RBD1 is a membrane-bound protein and its rubredoxin domain is on the stromal side of TM (Fig. 2*A*).

RBD1 Is Enriched in Stroma Lamellae Fractions of Both *Arabidopsis* and *Chlamydomonas* Where It Comigrates with PSII Monomers and Subcomplexes. We next investigated the localization of RBD1 using fractionated TM from *Arabidopsis*. These membranes were fractionated into grana core (GC), grana margins (GM), and stroma lamellae (SL). Each fraction was tested by SDS/PAGE and immunoblot analyses against known PSII assembly proteins ALB3 and HCF136, PSII subunit D2, PSI subunit PsaD, FNR, and RBD1 (Fig. 2*B*). RBD1, PsaD, ALB3, FNR, and HCF136 were clearly enriched in the SL fraction, whereas D2 was enriched in the GC fraction. We further performed BN-PAGE and immunoblot analyses of the native solubilized protein complexes from these fractionated membranes (*SI Appendix*, Fig. S2*A*). As expected, PSII-SC and LHCII trimers were enriched in GC membranes and were significantly reduced in SL membranes (40). As shown in *SI Appendix*, Fig. S2*A*, we found immunoblot signals for RBD1 comigrating with PSII-M, which occurred most strongly in the SL membrane fractions. These signals were also abundant in the LMW region of the 1D BN-PAGE, corresponding to protein complexes of low molecular mass, but also detached from protein complexes. To further explore protein–protein interactions between RBD1 and PSII subunits, we performed a coimmunoprecipitation (co-IP) experiment and mass spectrometry (MS) analyses from solubilized TM with specific anti-RBD1 and preimmune serum antibodies. The MS data clearly showed enrichment of RBD1 and PSII subunits peptides from 3 independent anti-RBD1 co-IP/MS experiments (*SI Appendix*, Table S2). These interactions were corroborated by immunoblot analyses, in which interactions between RBD1, Cyt b_{559} PsbE subunit, and D2 were verified (Fig. 2*C*, *Left*). In addition, we performed co-IP experiments with specific anti-PsbE and preimmune serum antibodies and solubilized protein complexes from *Arabidopsis* SL (Fig. 2*C*, *Right*). We confirmed the reciprocal co-IP of PsbE subunit together with RBD1 and D2 proteins, but not with the preimmune serum. These results were, similarly, reproduced in *Chlamydomonas* fractionated TM experiments, in which RBD1 protein was found comigrating with PSII monomers and PSII subcomplexes from SL membrane fractions (*SI Appendix*, Fig. S2 *B* and *C*). Interactions between RBD1 and PSII complexes were also studied in

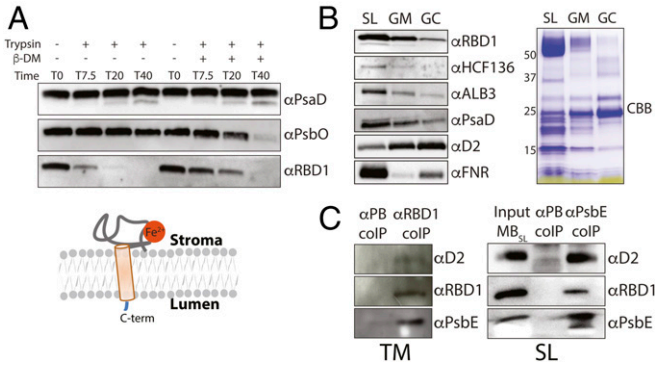

Fig. 2. *Arabidopsis* RBD1 rubredoxin domain faces the stromal side of the thylakoid membrane (TM), is enriched in stroma lamellae membrane fractions, and coimmunoprecipitates with the Cyt b_{559} and D2 subunits. (*A*) Effect of protease treatment on *Arabidopsis* TM. TM samples were incubated in the presence or in the absence (±) of trypsin (1 μg/mg Chl), as well as in the presence or absence (±) of β-DM, 0.25% (wt/vol), to solubilize membranes. SDS/PAGE and immunoblot analyses were performed from TM samples collected at 0, 7.5, 20, and 40 min of treatment. These samples were probed with antibodies against PsaD (an extrinsic PSI membrane protein on the stromal side), PsbO (an extrinsic PSII membrane protein on the luminal side), and RBD1. A schematic illustration of the RBD1 protein topology is also shown. (*B*) Denaturing SDS/PAGE and immunoblot analyses against D2, PsaD, ALB3, HCF136, FNR, and RBD1 from fractionated *Arabidopsis* TM. The lanes are labeled as follows: GC, grana core membranes; GM, grana margins membranes; SL, stroma lamellae membranes; TM, thylakoid membranes. (*C*) Co-IP experiments performed with β-DM–solubilized TM and SL protein complexes using antiserum specific for RBD1 (αRBD1) and the α-subunit of Cyt b_{559} (αPsbE), respectively. Input SL membrane loading corresponds to 0.2 μg of Chl, and a control co-IP was performed with preimmune serum (αPB).

Chlamydomonas from affinity-purified His-tagged CP47 (His47) PSII particles. As shown in *SI Appendix*, Fig. S2*D*, eluted His47 PSII particles exhibited high Chl *a* content and D2 immunoblot signals, but also contained enriched RBD1 proteins. A co-IP/MS experiment was performed with anti-RBD1 polyclonal antibodies from these samples, further confirming enrichment not only of RBD1 but also of PSII subunits, including both LMW subunits of the Cyt b_{559}. Notably, we also detected several low-abundance PSII assembly factors like Psb28, TEF30/MET1, and TL18 (*SI Appendix*, Table S3).

Dissection of the Roles of Membrane-Anchoring and Rubredoxin Domains of RBD1 in PSII Assembly and Repair. To delineate the role of the different protein domains necessary for the biological functions of *Chlamydomonas* RBD1 protein in PSII assembly and repair, we generated genetic constructs encoding mutated RBD1 proteins and evaluated whether these were able to complement the nonphotosynthetic and PSII-deficient phenotypes of the *2pac* mutant (Fig. 3*A*). We found that RBD1 constructs lacking either the chloroplast transit peptide (ΔTP) or the C-terminal TMH domain (ΔTMH) were unable to restore the photoautotrophic growth and PSII efficiency phenotypes of the mutant, as with the negative control transformation with GFP construct, despite normal accumulation of truncated RBD1 proteins (Fig. 3 *B* and *C* and *SI Appendix*, Fig. S4 *A*–*C*). These results confirm that RBD1 functions in the chloroplast, and they suggest an important role for the C-terminal TMH during de novo assembly of PSII.

Site-directed mutagenesis was performed to replace 2 out of the 4 cysteine residues that coordinate the iron atom of the rubredoxin domain (C76 and C109) with glycine (C76/109G), with the aim of altering iron binding and function (Fig. 3*A*). Interestingly, RBD1(C76/109G)-complemented lines were able to restore photoautotrophic growth, PSII efficiency, and PSII content under normal light conditions, similar to lines complemented with WT RBD1 (Fig. 3 *B*–*D*). We measured RBD1 protein content for 2 WT RBD1 and 2 RBD1(C76/109G)-complemented lines and compared these to the content of the WT 4A+ strain, from which the *2pac* mutant was generated (41). All tested lines exhibited greater RBD1 protein content than the 4A+ strain (Fig. 3*E*). The WT RBD1-complemented lines 1 and 2 exhibited 2- and 5-fold increments of RBD1 protein content, respectively, and the RBD1(C76/109G)-complemented lines 1 and 2 exhibited about 2-fold increments of RBD1 protein content (Fig. 3*E*).

We monitored changes in PSII efficiency from freshly grown TAP-agar plates under dark and very low light (~15 μmol photons·m^{-2}·s^{-1}) cycles on a 5-d time course with 5 WT and 8 C76/109G RBD1-complemented lines, 2 4A+, and the *2pac* mutant (Fig. 3*F*). Interestingly, we found that PSII efficiency declined with time in all studied RBD1(C76/109G) mutant lines, from an initial F_v/F_m of 0.56 ± 0.023 to final 0.26 ± 0.069, whereas both the WT RBD1-complemented lines and 4A+ strains did not exhibit significant changes in PSII efficiency (Fig. 3*F*).

We then monitored PSII efficiency from 5 WT and 5 RBD1(C76/109G)-complemented lines during exposure to 2 cycles of high-light (HL) treatments of 2 and 3 h duration each, interspersed with an overnight recovery period under very low light in the presence or absence of chloramphenicol (CAP) (Fig. 3*G*). CAP treatment inhibits chloroplast protein translation, thereby blocking the de novo assembly and repair of PSII. Interestingly, during the short HL treatments, we found that PSII efficiency declined faster and recovered more slowly in the RBD1(C76/109G) mutant background in comparison with WT RBD1 control lines (Fig. 3*G*). Alongside the reduction of PSII efficiency, higher F_o and F_m fluorescence parameters were measured in the mutant compared with WT RBD1 control lines (*SI Appendix*, Fig. S3*A*). CAP-treated cells exhibited similarly rapid reduction of PSII efficiency in both WT and RBD1(C76/109G) mutant under HL, in which PSII efficiency was abolished after 1 h and did not recover in these strains during the experiment (Fig. 3*G*). These results suggest an enhanced photoinhibition phenotype for RBD1(C76/109G), especially under HL. To test this further, we measured PSII-D1 protein content from whole cells treated with HL for 2 h in the presence and in the absence of CAP. RBD1(C76/109G)-complemented line exhibited enhanced D1 degradation upon HL treatment (Fig. 3*H* *and* *SI Appendix*, Fig. S3*B*). We found D2 protein content comparable in both complemented lines under these conditions. As expected, treatment of cells with HL and CAP led to fast degradation and no recovery for both D1 and D2 proteins, whereas the cellular content of acetylated tubulin was not affected (Fig. 3*H*). Notably, RBD1 protein content was not affected under HL or CAP treatments in both WT and RBD1(C76/109G) mutant lines in comparison with dark levels (Fig. 3*H*).

RBD1 Is a Redox-Active Protein That Participates in 1-Electron Transfer Reactions. Soluble rubredoxin proteins participate in 1-electron transfer reactions in many microbes (32, 42). Thus, the presence of the rubredoxin domain suggests that RBD1 may also participate in electron transfer reactions in TM. We therefore evaluated the spectroscopic, electrochemical, and electron transport properties of the rubredoxin domain of *Chlamydomonas* RBD1 (crRBD1). Recombinant crRBD1 lacking the predicted TP and the C-terminal TMH was reconstituted with Fe^{2+} anaerobically and further purified by anion exchange chromatography, as iron incorporation in the protein was minor after initial *E. coli* purification (Fig. 4*A*). The holoprotein was exceptionally pure, as only a single band corresponding to a protein with a molecular mass of 14.531 kDa was observed from SDS/PAGE and matrix-assisted laser desorption ionization–time of flight (MALDI-TOF) MS (Fig. 4*A* and *SI Appendix*, Fig. S5*A*), yielding about 80% iron (Fe^{2+}) content (Fig. 4*A*). The midpoint redox potential for

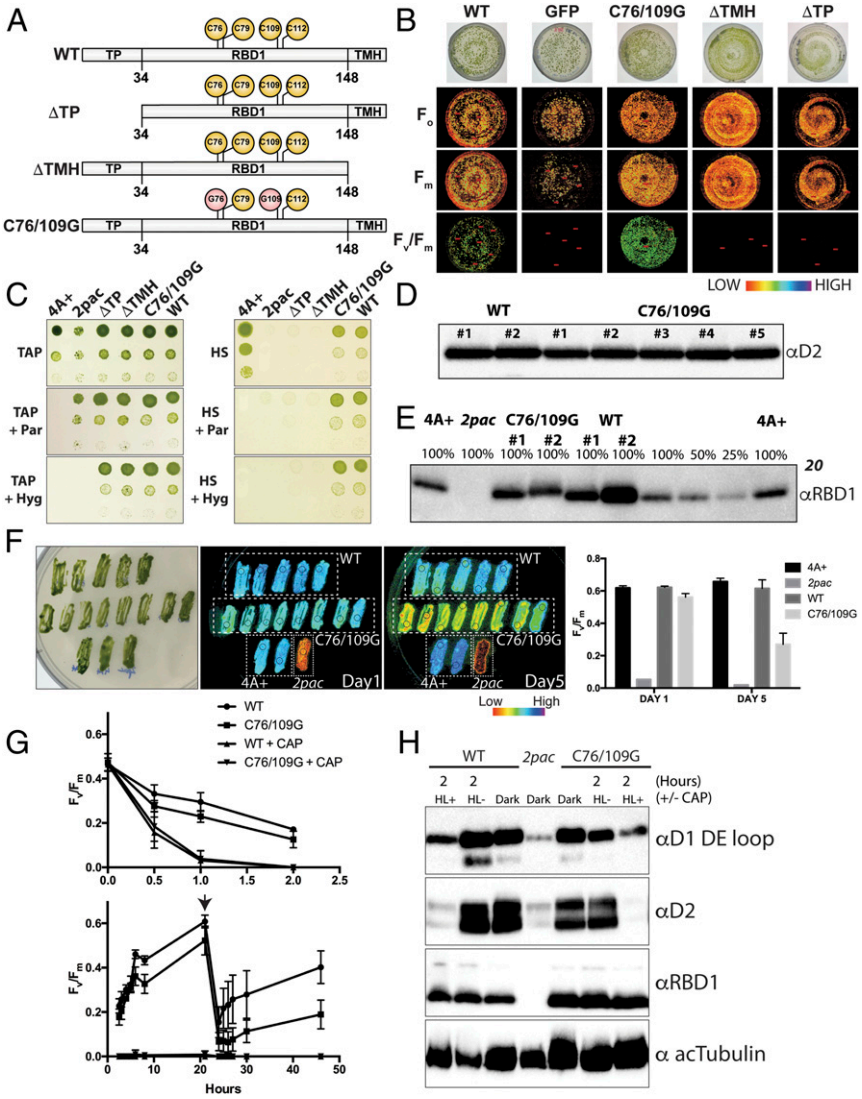

Fig. 3. Functional characterization of the different *Chlamydomonas* RBD1 protein domains. (*A*) Schematic diagrams of the truncated and amino acid substituted RBD1 proteins. Abbreviations are as follows: C76/109G, RBD1 with iron-coordinating cysteines 76 and 109 substituted to glycines; ΔTMH, RBD1 minus C-terminal α-helix transmembrane domain; ΔTP, RBD1 minus chloroplast transit peptide; WT, wild-type RBD1. (*B*) *2pac* complementation studies. Fluorescence parameters F_o, F_m, and PSII efficiency (F_v/F_m) measurements of hygromycin-resistant transformants obtained with constructs encoding for WT, the truncated proteins (ΔTP and ΔTMH), and the C76/109G substituted RBD1 proteins, as well as GFP. (*C*) Growth phenotypes of 4A+, *2pac* and WT, ΔTP, ΔTMH, and C76/109G RBD1-complemented lines. Cells were spotted onto HS and TAP solid media containing no antibiotics or 25 μg/mL of either paromomycin or hygromycin. Cells were grown under normal light growth conditions of 80 μmol photons·m^{-2}·s^{-1} for 1 wk. (*D*) Immunoblot analysis against D2 protein from whole-cell extracts of 2 WT and 5 C76/109G-complemented lines. (*E*) Immunoblot analysis against RBD1 protein from 4A+, *2pac*, and 2 WT, as well as 2 C76/109G-complemented lines whole cells (100% loading corresponds to 1.5×10^6 cells). (*F*) TAP grown C76/109G-complemented lines exhibit photoinhibition under low light growth conditions over time. PSII efficiency (F_v/F_m) was monitored for 5 d. (*G*) Photoinhibition studies of 5 WT and 5 C76/109G-complemented lines in the presence or absence of CAP (100 μg/mL). For measurements of PSII efficiency (F_v/F_m), cells were grown in the dark and subsequently transferred to a first round of HL (800 μmol photons·m^{-2}·s^{-1}) for 2 h (*Top*). Cells were then recovered under low light overnight. A second round of HL (indicated by an arrow) was performed for an additional 3 h, with further recovery under low light overnight (*Bottom*). (*H*) Immunoblot analyses against the D1 DE loop, D2, RBD1, and acetylated tubulin from dark grown and 2-h HL-incubated whole cells in the presence (+) or absence (–) of CAP. Loading corresponds to about 1.5×10^6 cells.

crRBD1 was determined to be +114 mV vs. AgCl/Ag (*SI Appendix*, Fig. S5 *B–D*). Spectroscopic analyses of holoproteins displayed characteristic UV/vis absorption spectra of native soluble rubredoxins (32, 33), with the expected charge-transfer bands corroborating the presence of a chelated iron. Upon exposure to oxygen, proteins were red in color and exhibited an absorption spectrum with peaks at 370 and 490 nm, with a shoulder at 570 nm (Fig. 4 *A* and *B*). Upon reduction, these absorption peaks disappeared, and the proteins became colorless (Fig. 4 *A* and *B*). We developed an assay for reduction of crRBD1 using spinach chloroplast-purified FNR and NADPH as an electron donor. The addition of both NADPH (250 μM) and FNR (1 μM) led to the rapid reduction of oxidized rubredoxins, whereas the addition of either NADPH or FNR alone did not (Fig. 4*B*). These results indicate that reduction of oxidized crRBD1 is NADPH dependent and is mediated by NADPH reductase activity.

To determine whether RBD1 is capable of 1-electron transfer reactions with heme-containing proteins, we tested whether RBD1 can transfer an electron to the heme *c* cofactor of cytochrome *c* (Cyt *c*). The equine heart Cyt *c* midpoint redox potential

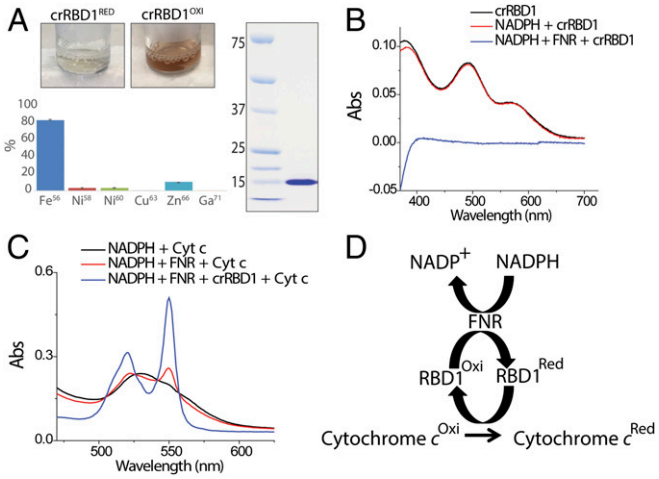

Fig. 4. Purification of the Fe^{2+} metal-substituted *Chlamydomonas* rubredoxin domain peptides (crRBD1) and determination of its electron carrier activity. (*A*) Image of purified peptides under reducing (crRBD1^{RED}) and oxidizing (crRBD1^{OXI}) conditions (*Top Left*). ICP-MS analysis of the percent of iron content following metal substitution (*Lower Left*). Coomassie-stained gel of ion exchange-purified Fe^{2+} metal-substituted rubredoxin domain proteins (loading corresponds to 10 μg of protein) (*Right*). (*B*) UV/vis absorption spectra of ambiently oxidized crRBD1 (Fe^{3+}) as well as NADPH- and FNR-reduced crRBD1 (Fe^{2+}) (90 μM). (*C*) Determination of electron carrier activity of the rubredoxin domain. Changes in the visible absorption spectra of the specific reduction of Cyt *c* by NADPH, FNR, and crRBD1 are evident. (*D*) Scheme for the NADPH–FNR–RBD1–Cyt *c* redox system. crRBD1 (5 μM) catalyzes the NADPH (0.25 mM)- and FNR (1 μM)-dependent reduction of Cyt *c* (50 μM).

is +250 mV vs. AgCl/Ag (43) and undergoes reduction that is air stable, thus serving as a convenient electron acceptor (44). Cyt *c* reduction was monitored by changes in the visible absorption spectrum at 550 nm. The soluble rubredoxin domain of RBD1 (5 μM) exhibited electron transfer to Cyt *c* (50 μM), which was NADPH and FNR dependent (Fig. 4 *C* and *D* and *SI Appendix*, Fig. S5*E*).

Discussion

RBD1 Is Involved in PSII Assembly and Repair in *Chlamydomonas*. In this study, we have taken advantage of the ability of *Chlamydomonas* to grow heterotrophically and assemble TM protein complexes in the dark, in addition to its genetic tractability, to gain information on the possible physiological roles of RBD1. PSI assembly takes place normally in the TM of the RBD1-deficient *2pac* mutant, whereas PSII macroorganization and PSII efficiency are drastically impaired compared with WT cells (Fig. 1 *A* and *C*), as observed previously (34). Only a minor accumulation of PSII-M complexes occurs in *2pac* TM in the dark (Fig. 1*D*), due to enhanced PSII-specific protein degradation rather than impaired chloroplast protein translation of PSII subunits (45).

Using 2 kinds of genetic constructs encoding mutated RBD1 proteins (Fig. 3*A*), we were able to dissect 2 different functions of RBD1 in PSII assembly and repair. First, the C-terminal TMH domain of RBD1 is essential for PSII de novo assembly, as *2pac* lines expressing the truncated RBD1 protein (ΔTMH-RBD1 mutant) were defective in both photoautotrophic growth and PSII efficiency (Fig. 3 *B* and *C* and *SI Appendix*, Fig. S4*C*). Second, the redox-active rubredoxin domain of RBD1 plays a critical role during PSII repair. Indeed, RBD1(C76/109G) mutant-complemented lines restore photoautotrophic growth and PSII efficiency under normal light. However, they are prone to enhanced photoinhibition under prolonged dark and low-light growth conditions, and also during short HL treatments (Fig. 3 *F–H* and *SI Appendix*, Fig. S3*B*).

Role of RBD1 in De Novo PSII Assembly. The data presented here demonstrate that RBD1 is strongly bound to TM and is enriched in SL fractions in both *Arabidopsis* and *Chlamydomonas* (Fig. 2*B* and *SI Appendix*, Figs. S1*B* and S2 *A–D*). These findings are consistent with the fact that SL are the sites where de novo assembly and repair of PSII complexes occur (46, 47). We also demonstrate the accumulation of RBD1 protein in a yellow-in-the-dark *Chlamydomonas* mutant, before light-dependent accumulation of PSII subunits (Fig. 1*E*). Interestingly, like RBD1, Cyt b_{559} and the PSII assembly factor HCF136 have also been reported to be synthesized before PSII RC subunits (30, 48), in agreement with the conservation of their respective genes in a gene cluster that is key to PSII biogenesis in cyanobacteria (29–31). Notably, our BN-PAGE and immunoblot analyses of solubilized SL membrane protein complexes in both *Chlamydomonas* and *Arabidopsis* clearly show that minor amounts of RBD1 protein comigrate with PSII-M and PSII subcomplexes, in agreement with previous findings (49), but not with PSII-D or PSII-SC (Fig. 1*D* and *SI Appendix*, Fig. S2 *A–D*). We find the majority of RBD1 at the front of the BN-PAGE, suggesting that RBD1 is either unassociated or detached from PSII complexes, possibly due to sample preparation, extraction during the detergent solubilization step, or dissociation during the BN-PAGE. Indeed, variation in the detection of PSII assembly factors in PSII RCs depending on the sample preparation has previously been reported (50). Importantly, we also show that RBD1 exhibits interactions with PSII subunits and PSII assembly factors, as shown by the enrichment of RBD1 with these proteins from co-IP/MS experiments in both *Arabidopsis* and *Chlamydomonas* (Fig. 2*C* and *SI Appendix*, Fig. S2*D* and Tables S2 and S3). Nonetheless, our results suggest that RBD1 is not a permanent component of the fully assembled PSII complex, but rather a transient one. This is supported by the latest cyanobacterial PSII crystal structure and by the plant PSII-SC structure, in which RBD1 is not present (51, 52).

Role of RBD1 in PSII Repair. PSII is constantly undergoing photooxidative damage and requires protective mechanisms to minimize it. Photoinhibition can occur at the PSII donor and acceptor sides (53). The former is thought to occur in PSII intermediate complexes lacking water-splitting activities that are undergoing assembly or repair processes. The protective pathway is thought to occur through slow electron transfer via the proximal β-carotene molecule (CarD2) to reduce highly oxidized Chl radicals in PSII ($P680^+$). This pathway requires the Cyt b_{559} redox properties of heme *b* 1-electron transfer activity to the β-carotene cation (25, 28, 54). Several questions remain about the electron source for this electron transfer pathway, but it has been suggested that oxidized Cyt b_{559} may accept an electron from the acceptor side of PSII (Q_B^-, or reduced PQH_2), thus forming a cyclic pathway of electron transfer within PSII (27, 28). Under conditions in which the plastoquinone pool is oxidized, such as during de novo assembly of PSII or under excessive PSII photoinhibition with demanding repair, an alternative electron source may be necessary. We hypothesize that the redox-active rubredoxin domain of RBD1 functions as an alternative electron donor to the Cyt b_{559} under assembly and repair conditions. The iron atom in all RBD1 orthologs exhibits conservation for the 2 cysteine canonical segments that are commonly found in prokaryotic rubredoxins (*SI Appendix*, Fig. S1*A*). It is thus likely that RBD1 participates in electron transfer reactions similarly to these ancient soluble rubredoxins (32, 33). These electron transfer pathways generally consist of a rubredoxin providing 1 electron to an enzyme and a rubredoxin reductase restoring an electron to the oxidized rubredoxin from a cofactor (e.g., NADPH) (33, 55). We also note that the functional role of the single redox-active rubredoxin domain of RBD1 is, necessarily, intermolecular, and clearly, interactions must take place on the

stromal side of the TMs (Fig. 2*A* and *SI Appendix*, Fig. S1*C*). The midpoint potential of the *Chlamydomonas* rubredoxin domain, +114 mV vs. AgCl/Ag (*SI Appendix*, Fig. S5 *B–D*), agrees with typical values measured for other rubredoxin proteins (−100 to +125 mV) (33, 49). Thus, electron transfer to the high potential form (HP) of Cyt b_{559}, with a midpoint redox potential of about +390 mV (24), is thermodynamically favorable. Moreover, we show that the rubredoxin domain of RBD1 is proficient for the 1-electron transfer reaction to heme *c* of the soluble Cyt *c* in vitro (Fig. 4 *C* and *D* and *SI Appendix*, Fig. S5*E*). We further demonstrate that reduction of oxidized RBD1 is NADPH and FNR dependent in vitro. Importantly, we find FNR enrichment in SL fractions (Fig. 2*B*), and previous studies have shown that FNR is membrane associated on the stromal side of TM protein complexes (56). Similarly, NADPH-dependent FNR activity has been described for the FNR/ferredoxin (Fd) redox system, in which NADPH is used to reduce Fd in nonphotosynthetic tissue of plants (57), in heterocysts of cyanobacteria (58), and in apicoplasts of apicomplexan parasites (59). These results suggest that FNR may act as a bona fide RBD1 reductase in the chloroplast, forming an FNR/RBD1/Cyt b_{559} redox system with NAPDH as source of alternative energized electrons.

Because the precise location of RBD1 in the PSII intermediate complexes is unknown, we can only speculate as to where it might be located and how interactions with PSII subunits might occur. The plant C2S2M2 PSII-SC structure obtained through single-particle cryo-electron microscopy (60) comprises a PSII dimeric core, as well as 2 strongly bound and 2 moderately bound LHCIIs. In this structure, both LMW subunits of the Cyt b_{559} (PsbE and PsbF) are located at the periphery of PSII complex and are not involved in the PSII monomer–monomer interface of the PSII dimer (C2) nor directly in contact with minor antenna subunits or LHCII trimers (60). We suggest that transient membrane protein–protein interactions might occur between the RBD1 single-spanning C-terminal TMH domain and LMW subunits of Cyt b_{559}, PsbE and PsbF, or proximal LMW subunits such as PsbY and PsbX (51, 60, 61), allowing the stromal rubredoxin domain of RBD1 (Fig. 2*A* and *SI Appendix*, Fig. S1*C*) to protrude on the acceptor side of PSII in the vicinity of the heme *b* cofactor of Cyt b_{559}.

The heme *b* is also facing the stromal side, slightly embedded in the protein matrix (23, 51). Indeed, protein docking experiments with fully assembled PSII complexes and RBD1 protein placed at the periphery of the Cyt b_{559} show that a distance of 29 Å may exist between the heme *b* group and the rubredoxin Fe^{2+} atom, hypothetically allowing for slow electron transport reactions (*SI Appendix*, Fig. S1*D*). It is worth mentioning that the distance between these cofactors may be different during PSII de novo assembly and repair conditions, in which dynamic changes in protein composition and complex structure are expected. In fact, there is ample evidence of additional PSII assembly factors that transiently bind to PSII (16). In this study, we demonstrate the presence of several of these low abundant PSII assembly factors from our co-IP/MS experiments, including TEF30/MET1, Psb28, and TLP18.3 (*SI Appendix*, Table S3). These interactions are of particular interest, as both TEF30/MET1 and Psb28, like the RBD1 rubredoxin domain, have been shown to interact with PSII intermediate complexes from the stromal side (62–64). Psb28 has been shown to interact with Cyt b_{559} by cross-linking experiments, and it has been proposed to participate in a mechanism that protects partially assembled PSII complexes from harmful redox back-reaction damage (62). *Arabidopsis* TEF30/MET1 has been suggested to function as a CP43/CP47 chaperone on the stromal side of the membrane during PSII assembly and repair (64), whereas the *Chlamydomonas* TEF30/MET1 ortholog has been proposed to be important during repair of PSII (63). TLP18.3 is a thylakoid luminal protein, and it is important during the repair cycle of PSII (65).

Taken together, based on published results and the genetic and biochemical data presented here, our results point to a role for RBD1 together with the Cyt b_{559} in a protective mechanism that minimizes damage of PSII complexes during repair. In the literature, 2 kinds of Cyt b_{559} mutants have been described. The first group includes null mutants targeting either of the 2 LMW subunits: PsbE and PsbF. Based on the study of these mutants, a clear role as a nucleation factor to initiate PSII assembly by forming a D2-Cyt b_{559} subcomplex that is strictly required for PSII biogenesis in oxygenic photosynthesis has been proposed (48, 66). The second group is composed of mutants with substituted amino acids that disrupt binding of the heme *b* cofactor (21–23, 67). In several cases, these mutants allow for the accumulation of apo-cytochrome b_{559} proteins and the residual assembly of oxygen evolving PSII complexes. Nevertheless, these were prone to photoinhibition under HL because of impaired repair (21, 22, 67). Thus, these 2 groups of mutants define a role for the Cyt b_{559} in the de novo assembly of PSII and the function of the redox heme *b* in the protection from photoinhibition. Phenotypically, the *Chlamydomonas 2pac* mutant exhibits PSII-deficient phenotypes (34, 48) similar to those of a null Cyt b_{559} mutant (34, 48), and moreover seem functionally connected, as both exhibit redox activity that is necessary to prevent photoinhibition. We suggest that the oxidized Cyt b_{559} is subsequently reduced by a stromal side NADPH–FNR–RBD1 redox system (Fig. 5). Furthermore, our results also suggest that RBD1, together with Cyt b_{559} and D2, might be a component of an early PSII subcomplex (RBD1–Cyt b_{559}–D2) that is involved in the stabilization, as a nucleation factor, of early PSII assembly complexes in photosynthetic eukaryotes (Fig. 5). This work not

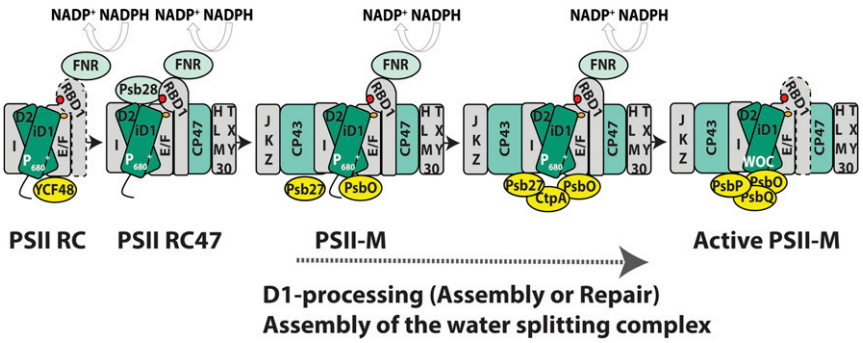

Fig. 5. Proposed model for the role of RBD1 during PSII assembly and repair in the chloroplast. We hypothesize that RBD1 (dashed line) together with Cyt b_{559} and D2 may form part of an early PSII subcomplex (RBD1–Cyt b_{559}–D2). The redox-active rubredoxin domain is stromal facing. This domain may deliver electrons from NADPH and FNR to Cyt b_{559} to protect the PSII assembly and repair intermediate complexes from photooxidative damage in stroma lamellae membranes.

only improves our understanding of cellular protection mechanisms for the vital PSII complex during assembly and repair but also informs genetic engineering strategies for oxidative protection of PSII to increase agricultural productivity.

Methods

Algal Strains and Growth Conditions. *Chlamydomonas* strains used in this study are WT 4A+ (*mt+*), *2pac* mutant (*mt+*) (34), His-tagged *psbB* (His47) (*mt+*) (68), and the yellow-in-the-dark mutant *chlL* (*mt+*) (37). Cells were grown heterotrophically or mixotrophically in Tris acetate-phosphate (TAP) medium (69) or photoautotrophically in high salt medium (70). Cell densities were determined with a Multisizer3 (Beckman Coulter). For photoinhibition studies, dark-grown cells were concentrated to about 2 to 3 $\times$ 10^7 cells·mL^{-1} in liquid TAP and incubated either under very LL or shifted to HL (800 μmol photons·m^{-2}·s^{-1}) for the indicated times in a temperature controlled (25 °C) HL chamber (Percival). TAP medium was supplemented with 100 μg/mL CAP or equivalent volume of 100% ethanol. Whole-cell samples were collected at different indicated time intervals for protein analyses. The PSII efficiency (71) was monitored by measuring the maximum quantum yield of PSII (F_v/F_m), determined after 15 min of dark adaptation, with a pulse-amplitude–modulated Chl fluorescence imaging system (MAXI-IMAGING-PAM; Heinz Walz).

Isolation of Thylakoid Membranes. *Chlamydomonas* cells were harvested by centrifugation at 2,500 $\times$ *g* for 10 min at 4 °C, followed by resuspension in lysis buffer (20 mM Hepes-KOH, pH 7.5, 5 mM $MgCl_2$) supplemented with protease inhibitor mixture cOmplete (Roche). Cells were disrupted by passage through a French press (SLM Aminco) at 10,000 psi at 4 °C. TMs were isolated by centrifugation at 20,500 $\times$ *g* for 10 min at 4 °C. Pelleted membranes were resuspended in TM buffer (20 mM Hepes-KOH, pH 7.5, 300 mM sorbitol, 10 mM KCl, and 5 mM $MgCl_2$).

Plant Growth and Chloroplast Isolation. *Arabidopsis* Columbia ecotype (Col-0) seedlings (WT) were grown on soil under 100 μmol photons·m^{-2}·s^{-1} with 10-h light/14-h dark conditions at 22 °C for 5 to 6 wk. Spinach leaves were obtained from a local market. For intact chloroplast isolation, plants were homogenized with an ULTRA-TURRAX disperser homogenizer (IKA) in chloroplast isolation buffer (20 mM Hepes-KOH, pH 8, 330 mM sorbitol, 10 mM EDTA, 10 mM $NaHCO_3$, and 5 mM $MgCl_2$). The homogenate was filtered through a double layer of Miracloth (Calbiochem) and collected in a prechilled Erlenmeyer flask. The obtained filtrate was centrifuged at 1,300 $\times$ *g* for 8 min at 4 °C to pellet intact chloroplasts. Pelleted chloroplasts were resuspended in resuspension buffer (20 mM Hepes-KOH, pH 8, 330 mM sorbitol, 10 mM $NaHCO_3$, and 5 mM $MgCl_2$) and loaded onto a premade, 40% and 75%, 2-step Percoll (GE Healthcare) gradient. Chloroplasts loaded onto the Percoll gradient were centrifuged at 1,500 $\times$ *g* in a swing-out rotor for 10 min at 4 °C, and chloroplasts were collected from the 40 to 75% green band intersection. Collected chloroplasts were diluted with 3 vol of resuspension buffer and further pelleted by centrifugation at 1,200 $\times$ *g* for 5 min at 4 °C. Chloroplast densities and intactness were determined with a Multisizer3 (Beckman Coulter). TMs from intact chloroplasts were isolated by lysing with hypoosmotic lysis buffer (20 mM Hepes/KOH, pH 8.0, 5 mM $MgCl_2$) and collected by centrifugation at 12,000 $\times$ *g*. Soluble stromal fractions were separated from pelleted thylakoids. Thylakoids were resuspended in storage buffer (20 mM Hepes-KOH, pH 8, 100 mM sorbitol, 10 mM $NaHCO_3$, and 5 mM $MgCl_2$). Chl determination was performed according to ref. 72.

Protein Topology Analyses. TMs were obtained from freshly isolated intact chloroplasts from spinach and *Arabidopsis* that were hypoosmotically lysed in the presence of 25 mM NH_4HCO_3. Intact and β-DM–solubilized (0.25% [wt/vol]) disrupted TMs were then incubated in the presence or in the absence of trypsin (1 μg/mg Chl). Immunoblot analyses were performed from collected TM samples after 0, 7.5, 20, and 40 min of protease treatment and were probed with antibodies directed against PsaD, PsbO, and RBD1 proteins.

TM Subfractionation. TMs were fractionated into grana, grana margins, and stroma lamellae membrane fractions by digitonin detergent solubilization followed by differential centrifugation, as modified from published protocols (40, 73). In brief, TMs at a final concentration of 0.2 mg Chl·mL^{-1} in a buffer containing 15 mM Tricine-KOH, pH 7.9, 0.1 M sorbitol, 10 mM NaCl, and 5 mM $MgCl_2$ were solubilized with a final concentration of 0.2% digitonin (wt/vol) (Sigma-Aldrich) by gentle pipetting, followed by incubation for 5 min at room temperature. The mixture was centrifuged at 1,000 $\times$ *g* for 10 min at 4 °C to pellet insoluble material. The remaining suspension was further centrifuged at 10,000 $\times$ *g* for 30 min, 40,000 $\times$ *g* for 60 min, and 150,000 $\times$ *g* for 90 min at 4 °C. The pelleted membranes from each centrifugation step correspond to grana (GC), grana margins (GM), and stroma lamellae (SL), respectively. Membranes were diluted with 10% glycerol and stored at −20 °C. The Chl content was determined by published methods (72). The Chl *a*/*b* ratio was measured for each *Arabidopsis* fraction to be 3.7 ± 0.02 (TM), 2.7 ± 0.02 (GC), 4.7 ± 0.06 (GM), and 9.6 ± 0.27 (SL).

BN-PAGE. BN-PAGE analyses were performed as previously described (40, 74). In brief, solubilization of TMs and fractionated membranes were concentrated to 1 mg/mL Chl and solubilized with equal volumes of 2% β-DM or α-DM (Anatrace) detergents as indicated, yielding 0.5 mg Chl·mL^{-1} and 1% detergent final concentrations. Solubilized samples were loaded onto a precast Native-PAGE 4 to 16% Bis Tris (Invitrogen) and separated at 4 °C.

SDS/PAGE and Immunoblot Analysis. Immunoblot analyses were performed as previously described (75). Loading of samples was based on either an equal Chl or protein basis, as indicated. Denatured proteins were resolved in precast 10 to 20% gradient SDS/PAGE (Invitrogen) and transferred to polyvinylidene difluoride membranes (Immobilon-FL; 0.45 μm; Millipore) in a tank electrotransfer system. Polyclonal antibodies against D2, D1, PsbO, PsbE, CP43, and PsaD were obtained from Agrisera, Sweden, and ALB3 from D.S. The antibody against HCF136 was a kind gift from Karin Meierhoff, Heinrich-Heine-Universität Düsseldorf, Germany. Polyclonal antibodies against *Chlamydomonas* and *Arabidopsis* RBD1 proteins were generated and described in published procedures (34). Immunoblot signals were visualized by Supersignal West Pico Chemiluminescent substrate detection system (Thermo Fisher Scientific) in a ChemiDoc MP imager and quantitated with Image Lab, version 3.0 (Bio-Rad).

Co-IP. TM- and SL-enriched fractions at a Chl concentration of 1 mg/mL were solubilized with an equal volume of a solution containing 2% β-DM in 1× PBS buffer, on ice for 5 min. Solubilized membranes were subsequently centrifuged for 1 min at 20,500 $\times$ *g* at 4 °C to remove insolubilized material. One volume of solubilized supernatant was then combined with an equal volume of 1× PBS buffer containing 10 μL of either specific polyclonal rabbit anti-RBD1, anti-PsbE antibodies (Agrisera), or rabbit preimmune serum antibodies as negative control. Solubilized membranes and antibodies were incubated for 1 h at 4 °C with constant rocking. Subsequently, 50 μL of 1× PBS buffer-washed Agarose IP trueblot beads (Rockland) were added to the solution of solubilized membrane protein complexes and antibodies and incubated for 2 h at 4 °C with constant rocking. Agarose IP trueblot beads were centrifuged at 2,600 $\times$ *g* for 1 min at 4 °C and washed 3× with 1 mL of 1× PBS/0.2% β-DM followed with 1 wash with 1× PBS/0.03% β-DM. The supernatant was removed completely. Pelleted Agarose IP trueblot beads were solubilized at 60 °C for 30 min with 30 μL of 2× SDS denaturing solution (0.2 M Tris, pH 6.8, 4% SDS, 2 M urea, 1 mM EDTA, and 20% glycerol) supplemented with 5% final volume of β-mercaptoethanol. Solubilized proteins were loaded onto a gradient 10 to 20% SDS/PAGE gel (Invitrogen). Separated peptides were sliced from the SDS/PAGE, in-gel-digested, and analyzed by MS following the method described by the Vincent J. Coates Proteomics/Mass Spectrometry Laboratory.

Cloning, Protein Purification, and Metal Substitution. Primers are listed in *SI Appendix*, Table S1. The *Arabidopsis* full-length RBD1 cDNA (gene At1g54500) was obtained from TAIR, clone U12560. *Chlamydomonas* RNA isolation, reverse transcriptase PCR, and cDNA synthesis were performed as described in published protocols (76). PCR products amplified for the *Chlamydomonas* RBD1 cDNA (gene Cre07.g315150) were cloned into pJet 1.2 (CloneJET PCR Cloning Kit; Thermo Fisher Scientific) and sequenced. Recombinant His-tagged rubredoxin domain proteins were expressed and purified as described in published protocols (77). Briefly, cDNA encoding the *Chlamydomonas* RBD1 proteins, lacking the predicted N-terminal chloroplast TP (amino acids Met-1 to Val-34) and the C-terminal TMH membrane anchoring domain (amino acids Gly-149 to Glu-169) were PCR amplified using forward and reverse primers that included NdeI and BamHI restriction sites, respectively. PCR products were NdeI and BamHI restriction enzyme-digested and subcloned into pET28 (a+) (Novagen). For the production of RBD1 recombinant protein, *E. coli* BL21 (DE3) (Novagen) cells at OD_{600} of 0.6 were induced with 0.25 mM isopropyl β-D-thiogalactoside at 37 °C for 3 h. Cells were sedimented by centrifugation at 20,500 $\times$ *g* for 15 min at 4 °C and disrupted with a French press (20,000 psi). Disrupted cells were centrifuged at 20,500 $\times$ *g* for 15 min at 4 °C to separate the supernatant. His-tagged proteins were affinity purified from the supernatant, under native conditions with Ni-NTA agarose (Qiagen) following the manufacturer's instructions. Metal substitution steps were carried out in a nitrogen and hydrogen

(less than 2%) atmosphere glove box, with levels of oxygen less than 10 ppm (Coy Laboratories). Briefly, affinity-purified recombinant RBD1 proteins were incubated in the presence of 0.5 M DTT for 5 min before being precipitated by addition of trichloroacetic acid at a final concentration of 5%. The protein precipitant was pelleted by centrifugation at 5,000 × *g* for 5 min, and the supernatant was discarded. The pelleted protein was subsequently resuspended by pipetting in a solution of 0.5 M Tris·HCl, pH 8.0, followed by the addition of a solution containing a 2.5-fold molar excess of $FeSO_4$ $7H_2O$. The protein was allowed to incubate with the metal salt at room temperature for 1 h. The reconstituted protein was further centrifuged at 20,500 × *g* for 5 min to pellet any remaining metal adduct precipitant. Metal-substituted rubredoxin proteins were further purified by ion exchange chromatography with a Hitrap Q HP column (GE Healthcare), operated with a peristaltic pump in the anaerobic glove box. The protein was loaded onto the column in solution of 25 mM Tris·HCl, pH 8.0, washed with a 10-column bed volume and eluted with a 4-column bed volume of the same buffer containing 0.2 M NaCl. Eluted protein fractions were pooled and further concentrated with Amicon ultra centrifugal filters (Millipore) with a 10-kDa cutoff. Proteins were quantified by the DC protein assay (Bio-Rad) and by measuring the protein absorption at 280 nm with a Nanodrop (Thermo Fisher Scientific). Protein purity was verified by denaturing SDS/PAGE Coomassie blue staining analyses and MALDI-TOF MS analyses. Iron content was determined by inductively coupled plasma mass spectrometry (ICP-MS) as described in published protocols (78). Proteins were diluted to 5 μM and metal content analyses were performed by ICP-MS containing known amounts of gallium as internal control.

Mutant Complementation Studies. The *Chlamydomonas 2pac* mutant was generated via DNA insertional mutagenesis as described in ref. 41, conferring paromomycin antibiotic resistance. The RBD1 cDNA containing cysteine residues Cys-76 and Cys-109 mutated to glycine were obtained from gblocks (IDT). Truncation of TP (Met-1 to Val-34) and TMH (Gly-149 to Asp-169) were generated by PCR amplification from RBD1 WT cDNA. Amplification of WT and mutated constructs included NdeI and XbaI restriction enzyme sites that were used to clone into pJG, a modified pSL18 plasmid (79). This plasmid is composed of the PsaD promotor and terminator (80), as well as a hygromycin resistance cassette instead of aphVIII. GFP was cloned by NdeI and XbaI restriction enzyme digestion into pJG as a negative control. *Chlamydomonas 2pac* transformation was performed by electroporation from logarithmic-phase grown cells resuspended with MAX Efficiency transformation medium according to the manufacturer's instructions (Thermo Fisher Scientific). *Chlamydomonas* transformants were selected on TAP plates containing 25 μg/mL hygromycin (Invitrogen) or paromomycin (Sigma).

NADPH and FNR-Dependent Rubredoxin Reduction Measurement. The rubredoxin domain protein (90 μM) reduction assay was measured in a reaction mixture (100 μL) containing 20 mM Tris·HCl, pH 8.0, 1 μM ferredoxin NADPH reductase (FNR), and 250 μM NADPH (Roche). Spinach chloroplast-purified ferredoxin $NADP^+$ reductase and anti-FNR antibodies were kindly donated by R. Malkin, University of California, Berkeley, CA. The reaction was monitored in a 96-well plate with a UV transparent flat bottom (Corning) with TECAM Infinity 2000 plate reader by measuring absorption spectra from 350 to 700 nm. Equine heart Cyt *c* was purchased from Sigma-Aldrich. Cyt *c* reduction (50 μM) was measured by changes in absorbance at 550 nm in a reaction mixture (100 μL) containing 20 mM Tris·HCl, pH 8.0, 1 μM FNR, and 250 μM NADPH (Roche) in the presence or absence of rubredoxin domain proteins (5 μM). Reactions were started by the addition of NADPH, and the increase in A_{550} due to the reduction of Cyt *c* was measured and followed for 125 s.

Transmission Electron Microscopy. For cell fixation, 7 mL of cell culture was supplemented with 1 mL of 8% glutaraldehyde and put on rocker for 1 min. Another 1 mL of aqueous 2% osmium tetroxide and 1.5% potassium ferricyanide was added, and the solution was rocked for 7 min. Cells were spun down at 2,500 × *g* for 1 min, the supernatant containing fixatives was discarded, and the pellet containing the cells was washed 3 times with distilled water. The final resuspended pellet was warmed to 37 °C for 5 min, complemented with 1 vol of 2% low melting agarose at 37 °C, centrifuged at 20,500 × *g* for 10 s, and cooled to 4 °C until processing. After 3 washes with distilled water, the cell pellet was cut into pieces (1 mm^3), dehydrated using increasing concentrations of acetone for 5 min (25%, 35%, 50%, 70%, 75%, and 95%), and left in pure acetone for 15 min. For infiltration, cell pellets were incubated for 15 min with increasing concentrations of 25%, 50%, and 75% acetone/Epon resin mixture and rotation. Cells were sedimented at 2,500 × *g* between changes, followed by a final 3 changes for 10 min each in pure Epon resin. Finally, samples were placed in BEEM capsules for polymerization at 60 °C for 2 d. Ultrathin sections (60 to 70 nm) were cut with a diamond knife (Diatome; type ultra 358) on an EM UC6 μLtramicrotome (Leica) and mounted on single-slot Pioloform-coated copper grids (Plano). Subsequently, sections were stained with uranyl acetate and lead citrate and viewed with an EM 902A (Carl Zeiss) transmission electron microscope (both operated at 80 kV). Micrographs were taken using a 4,080 × 4,080-pixel or 1,350 × 1,040-pixel charge-coupled device camera (UltraScan 4000 or Erlangshen ES500W, respectively; Gatan) and Gatan Digital Micrograph software (version 1.70.16). Image brightness and contrast were adjusted, and figures were assembled using Adobe Photoshop 8.0.1.

ACKNOWLEDGMENTS. We are grateful to Christopher Gee and Sheila McCormick for critical reading of the manuscript. We thank John D. Coates for access to an anaerobic glove box, Andrew Hagen for technical help with the in silico protein docking analyses, and Tyler Detomasi and Christopher J. Chang for technical help with ICP-MS analyses. We also thank the A. O. Beckman Postdoctoral Fellowship for funding A.L.F. K.K.N. is an investigator of the Howard Hughes Medical Institute.

1. N. Nelson, C. F. Yocum, Structure and function of photosystems I and II. *Annu. Rev. Plant Biol.* **57**, 521–565 (2006).
2. D. J. Vinyard, G. M. Ananyev, G. C. Dismukes, Photosystem II: The reaction center of oxygenic photosynthesis. *Annu. Rev. Biochem.* **82**, 577–606 (2013).
3. K. J. van Wijk, M. Roobol-Boza, R. Kettunen, B. Andersson, E. M. Aro, Synthesis and assembly of the D1 protein into photosystem II: Processing of the C-terminus and identification of the initial assembly partners and complexes during photosystem II repair. *Biochemistry* **36**, 6178–6186 (1997).
4. A. Rokka, M. Suorsa, A. Saleem, N. Battchikova, E. M. Aro, Synthesis and assembly of thylakoid protein complexes: Multiple assembly steps of photosystem II. *Biochem. J.* **388**, 159–168 (2005).
5. O. Nanba, K. Satoh, Isolation of a photosystem II reaction center consisting of D-1 and D-2 polypeptides and cytochrome *b*-559. *Proc. Natl. Acad. Sci. U.S.A.* **84**, 109–112 (1987).
6. L. X. Shi, M. Hall, C. Funk, W. P. Schröder, Photosystem II, a growing complex: Updates on newly discovered components and low molecular mass proteins. *Biochim. Biophys. Acta* **1817**, 13–25 (2012).
7. B. A. Diner, D. F. Ries, B. N. Cohen, J. G. Metz, COOH-terminal processing of polypeptide D1 of the photosystem II reaction center of *Scenedesmus obliquus* is necessary for the assembly of the oxygen-evolving complex. *J. Biol. Chem.* **263**, 8972–8980 (1988).
8. J. L. Roose, H. B. Pakrasi, Evidence that D1 processing is required for manganese binding and extrinsic protein assembly into photosystem II. *J. Biol. Chem.* **279**, 45417–45422 (2004).
9. N. Keren, A. Berg, P.J. van Kan, H. Levanon, I. Ohad, Mechanism of photosystem II photoinactivation and D1 protein degradation at low light: The role of back electron flow. *Proc. Natl. Acad. Sci. U.S.A.* **94**, 1579–1584 (1997).
10. E. M. Aro, I. Virgin, B. Andersson, Photoinhibition of Photosystem II. Inactivation, protein damage and turnover. *Biochim. Biophys. Acta* **1143**, 113–134 (1993).
11. A. Melis, Photosystem-II damage and repair cycle in chloroplasts: What modulates the rate of photodamage? *Trends Plant Sci.* **4**, 130–135 (1999).
12. I. Ohad, D. J. Kyle, C. J. Arntzen, Membrane protein damage and repair: Removal and replacement of inactivated 32-kilodalton polypeptides in chloroplast membranes. *J. Cell Biol.* **99**, 481–485 (1984).
13. N. Adir, H. Zer, S. Shochat, I. Ohad, Photoinhibition—a historical perspective. *Photosynth. Res.* **76**, 343–370 (2003).
14. P. J. Nixon, F. Michoux, J. Yu, M. Boehm, J. Komenda, Recent advances in understanding the assembly and repair of photosystem II. *Ann. Bot.* **106**, 1–16 (2010).
15. J. Nickelsen, B. Rengstl, Photosystem II assembly: From cyanobacteria to plants. *Annu. Rev. Plant Biol.* **64**, 609–635 (2013).
16. Y. Lu, Identification and roles of photosystem II assembly, stability, and repair factors in *Arabidopsis*. *Front. Plant Sci.* **7**, 168 (2016).
17. T. Cardona, A. Sedoud, N. Cox, A. W. Rutherford, Charge separation in photosystem II: A comparative and evolutionary overview. *Biochim. Biophys. Acta* **1817**, 26–43 (2012).
18. Y. Nishiyama *et al*., Oxidative stress inhibits the repair of photodamage to the photosynthetic machinery. *EMBO J.* **20**, 5587–5594 (2001).
19. I. Vass *et al*., Reversible and irreversible intermediates during photoinhibition of photosystem II: Stable reduced QA species promote chlorophyll triplet formation. *Proc. Natl. Acad. Sci. U.S.A.* **89**, 1408–1412 (1992).
20. R. Kale *et al*., Amino acid oxidation of the D1 and D2 proteins by oxygen radicals during photoinhibition of Photosystem II. *Proc. Natl. Acad. Sci. U.S.A.* **114**, 2988–2993 (2017).
21. F. Morais *et al*., Photosynthetic water oxidation in cytochrome b_{559} mutants containing a disrupted heme-binding pocket. *J. Biol. Chem.* **276**, 31986–31993 (2001).
22. M. Sugiura, M. Nakamura, K. Koyama, A. Boussac, Assembly of oxygen-evolving Photosystem II efficiently occurs with the apo-Cytb_{559} but the holo-Cytb_{559} accelerates the recovery of a functional enzyme upon photoinhibition. *Biochim. Biophys. Acta* **1847**, 276–285 (2015).

23. H. B. Pakrasi, P. De Ciechi, J. Whitmarsh, Site directed mutagenesis of the heme axial ligands of cytochrome b_{559} affects the stability of the photosystem II complex. *EMBO J.* **10**, 1619–1627 (1991).
24. M. Roncel *et al*., Redox properties of the photosystem II cytochromes b_{559} and c_{550} in the cyanobacterium *Thermosynechococcus elongatus*. *J. Biol. Inorg. Chem.* **8**, 206–216 (2003).
25. P. Faller, A. Pascal, A. W. Rutherford, Beta-carotene redox reactions in photosystem II: Electron transfer pathway. *Biochemistry* **40**, 6431–6440 (2001).
26. C. A. Tracewell, G. W. Brudvig, Characterization of the secondary electron-transfer pathway intermediates of photosystem II containing low-potential cytochrome b_{559}. *Photosynth. Res.* **98**, 189–197 (2008).
27. H. A. Chu, Y. F. Chiu, The roles of cytochrome b_{559} in assembly and photoprotection of photosystem II revealed by site-directed mutagenesis studies. *Front. Plant Sci.* **6**, 1261 (2016).
28. K. E. Shinopoulos, G. W. Brudvig, Cytochrome b_{559} and cyclic electron transfer within photosystem II. *Biochim. Biophys. Acta* **1817**, 66–75 (2012).
29. S. A. Jackson, J. R. Hervey, A. J. Dale, J. J. Eaton-Rye, Removal of both Ycf48 and Psb27 in *Synechocystis* sp. PCC 6803 disrupts Photosystem II assembly and alters Q(A)(–) oxidation in the mature complex. *FEBS Lett.* **588**, 3751–3760 (2014).
30. J. Meurer, H. Plücken, K. V. Kowallik, P. Westhoff, A nuclear-encoded protein of prokaryotic origin is essential for the stability of photosystem II in *Arabidopsis thaliana*. *EMBO J.* **17**, 5286–5297 (1998).
31. M. Suorsa *et al*., Protein assembly of photosystem II and accumulation of subcomplexes in the absence of low molecular mass subunits PsbL and PsbJ. *Eur. J. Biochem.* **271**, 96–107 (2004).
32. W. Lovenberg, B. E. Sobel, Rubredoxin: A new electron transfer protein from *Clostridium pasteurianum*. *Proc. Natl. Acad. Sci. U.S.A.* **54**, 193–199 (1965).
33. J.-M. M. Jacques Meyer "Rubredoxin" in *Encyclopedia of Inorganic and Bioinorganic Chemistry*, R. A. Scott, Ed. (Wiley, 2011).
34. R. H. Calderon *et al*., A conserved rubredoxin is necessary for photosystem II accumulation in diverse oxygenic photoautotrophs. *J. Biol. Chem.* **288**, 26688–26696 (2013).
35. B. L. Gutman, "DNA repair in the chloroplast," PhD thesis, University of California, Berkeley (2007).
36. I. Ohad, P. Siekevitz, G. E. Palade, Biogenesis of chloroplast membranes. II. Plastid differentiation during greening of a dark-grown algal mutant (*Chlamydomonas reinhardi*). *J. Cell Biol.* **35**, 553–584 (1967).
37. A. B. Cahoon, M. P. Timko, *yellow-in-the-dark* mutants of *Chlamydomonas* lack the CHLL subunit of light-independent protochlorophyllide reductase. *Plant Cell* **12**, 559–568 (2000).
38. A. Szczepaniak, D. Huang, T. W. Keenan, W. A. Cramer, Electrostatic destabilization of the cytochrome b_6f complex in the thylakoid membrane. *EMBO J.* **10**, 2757–2764 (1991).
39. A. L. Zilber, R. Malkin, Organization and topology of photosystem I subunits. *Plant Physiol.* **99**, 901–911 (1992).
40. S. Järvi, M. Suorsa, V. Paakkarinen, E. M. Aro, Optimized native gel systems for separation of thylakoid protein complexes: Novel super- and mega-complexes. *Biochem. J.* **439**, 207–214 (2011).
41. R. M. Dent *et al*., Large-scale insertional mutagenesis of *Chlamydomonas* supports phylogenomic functional prediction of photosynthetic genes and analysis of classical acetate-requiring mutants. *Plant J.* **82**, 337–351 (2015).
42. F. Auchère *et al*., Overexpression and purification of *Treponema pallidum* rubredoxin; kinetic evidence for a superoxide-mediated electron transfer with the superoxide reductase neelaredoxin. *J. Biol. Inorg. Chem.* **9**, 839–849 (2004).
43. Y. P. Myer, A. F. Saturno, B. C. Verma, A. Pande, Horse heart cytochrome *c*. The oxidation-reduction potential and protein structures. *J. Biol. Chem.* **254**, 11202–11207 (1979).
44. J. H. Capdevila *et al*., Cytochrome P-450 enzyme-specific control of the regio- and enantiofacial selectivity of the microsomal arachidonic acid epoxygenase. *J. Biol. Chem.* **265**, 10865–10871 (1990).
45. R. H. Calderon, "Genetic and biochemical studies of photosystem II assembly," PhD thesis, University of California, Berkeley (2015).
46. S. Puthiyaveetil *et al*., Compartmentalization of the protein repair machinery in photosynthetic membranes. *Proc. Natl. Acad. Sci. U.S.A.* **111**, 15839–15844 (2014).
47. S. Järvi, M. Suorsa, E. M. Aro, Photosystem II repair in plant chloroplasts–Regulation, assisting proteins and shared components with photosystem II biogenesis. *Biochim. Biophys. Acta* **1847**, 900–909 (2015).
48. F. Morais, J. Barber, P. J. Nixon, The chloroplast-encoded alpha subunit of cytochrome b_{559} is required for assembly of the photosystem two complex in both the light and the dark in *Chlamydomonas reinhardtii*. *J. Biol. Chem.* **273**, 29315–29320 (1998).
49. J. Wastl *et al*., Eukaryotically encoded and chloroplast-located rubredoxin is associated with photosystem II. *J. Biol. Chem.* **275**, 30058–30063 (2000).
50. J. Komenda *et al*., The cyanobacterial homologue of HCF136/YCF48 is a component of an early photosystem II assembly complex and is important for both the efficient assembly and repair of photosystem II in *Synechocystis* sp. PCC 6803. *J. Biol. Chem.* **283**, 22390–22399 (2008).
51. Y. Umena, K. Kawakami, J. R. Shen, N. Kamiya, Crystal structure of oxygen-evolving photosystem II at a resolution of 1.9 Å. *Nature* **473**, 55–60 (2011).
52. X. Wei *et al*., Structure of spinach photosystem II-LHCII supercomplex at 3.2 Å resolution. *Nature* **534**, 69–74 (2016).
53. I. Vass, Molecular mechanisms of photodamage in the Photosystem II complex. *Biochim. Biophys. Acta* **1817**, 209–217 (2012).
54. A. Telfer, Too much light? How beta-carotene protects the photosystem II reaction centre. *Photochem. Photobiol. Sci.* **4**, 950–956 (2005).
55. F. E. Jenney, Jr, M. F. Verhagen, X. Cui, M. W. Adams, Anaerobic microbes: Oxygen detoxification without superoxide dismutase. *Science* **286**, 306–309 (1999).
56. J. P. Benz *et al*., *Arabidopsis* Tic62 and ferredoxin-NADP(H) oxidoreductase form light-regulated complexes that are integrated into the chloroplast redox poise. *Plant Cell* **21**, 3965–3983 (2009).
57. Y. Onda *et al*., Differential interaction of maize root ferredoxin:NADP(+) oxidoreductase with photosynthetic and non-photosynthetic ferredoxin isoproteins. *Plant Physiol.* **123**, 1037–1045 (2000).
58. A. M. Weber-Main *et al*., An electrochemical, kinetic, and spectroscopic characterization of [2Fe-2S] vegetative and heterocyst ferredoxins from *Anabaena* 7120 with mutations in the cluster binding loop. *Arch. Biochem. Biophys.* **355**, 181–188 (1998).
59. M. Vollmer, N. Thomsen, S. Wiek, F. Seeber, Apicomplexan parasites possess distinct nuclear-encoded, but apicoplast-localized, plant-type ferredoxin-NADP$^+$ reductase and ferredoxin. *J. Biol. Chem.* **276**, 5483–5490 (2001).
60. X. Su *et al*., Structure and assembly mechanism of plant $C_2S_2M_2$-type PSII-LHCII supercomplex. *Science* **357**, 815–820 (2017).
61. K. Kawakami, M. Iwai, M. Ikeuchi, N. Kamiya, J. R. Shen, Location of PsbY in oxygen-evolving photosystem II revealed by mutagenesis and X-ray crystallography. *FEBS Lett.* **581**, 4983–4987 (2007).
62. D. A. Weisz *et al*., Mass spectrometry-based cross-linking study shows that the Psb28 protein binds to cytochrome b_{559} in Photosystem II. *Proc. Natl. Acad. Sci. U.S.A.* **114**, 2224–2229 (2017).
63. L. S. Muranaka *et al*., TEF30 interacts with photosystem II monomers and is involved in the repair of photodamaged photosystem II in *Chlamydomonas reinhardtii*. *Plant Physiol.* **170**, 821–840 (2016).
64. N. H. Bhuiyan, G. Friso, A. Poliakov, L. Ponnala, K. J. van Wijk, MET1 is a thylakoid-associated TPR protein involved in photosystem II supercomplex formation and repair in *Arabidopsis*. *Plant Cell* **27**, 262–285 (2015).
65. S. Sirpiö *et al*., TLP18.3, a novel thylakoid lumen protein regulating photosystem II repair cycle. *Biochem. J.* **406**, 415–425 (2007).
66. J. Komenda *et al*., Accumulation of the D2 protein is a key regulatory step for assembly of the photosystem II reaction center complex in *Synechocystis* PCC 6803. *J. Biol. Chem.* **279**, 48620–48629 (2004).
67. M. L. Hamilton *et al*., Investigating the photoprotective role of cytochrome b_{559} in photosystem II in a mutant with altered ligation of the haem. *Plant Cell Physiol.* **55**, 1276–1285 (2014).
68. T. Suzuki *et al*., Binding and functional properties of the extrinsic proteins in oxygen-evolving photosystem II particle from a green alga, *Chlamydomonas reinhardtii* having his-tagged CP47. *Plant Cell Physiol.* **44**, 76–84 (2003).
69. E. H. Harris, *The Chlamydomonas Sourcebook: A Comprehensive Guide to Biology and Laboratory Use* (Academic, San Diego, 1989).
70. N. Sueoka, Mitotic replication of deoxyribonucleic acid in *Chlamydomonas reinhardi*. *Proc. Natl. Acad. Sci. U.S.A.* **46**, 83–91 (1960).
71. K. Maxwell, G. N. Johnson, Chlorophyll fluorescence—a practical guide. *J. Exp. Bot.* **51**, 659–668 (2000).
72. R. J. Porra, W. A. Thompson, P. E. Kriedemann, Determination of accurate extinction coefficients and simultaneous-equations for assaying chlorophyll-a and chlorophyll-B extracted with 4 different solvents—verification of the concentration of chlorophyll standards by atomic-absorption spectroscopy. *Biochim. Biophys. Acta* **975**, 384–394 (1989).
73. F. Ossenbühl, K. Hartmann, J. Nickelsen, A chloroplast RNA binding protein from stromal thylakoid membranes specifically binds to the 5′ untranslated region of the psbA mRNA. *Eur. J. Biochem.* **269**, 3912–3919 (2002).
74. J. G. García-Cerdán *et al*., The PsbW protein stabilizes the supramolecular organization of photosystem II in higher plants. *Plant J.* **65**, 368–381 (2011).
75. J. G. García-Cerdán *et al*., Antisense inhibition of the PsbX protein affects PSII integrity in the higher plant *Arabidopsis thaliana*. *Plant Cell Physiol.* **50**, 191–202 (2009).
76. P. T. Tran, M. N. Sharifi, S. Poddar, R. M. Dent, K. K. Niyogi, Intragenic enhancers and suppressors of phytoene desaturase mutations in *Chlamydomonas reinhardtii*. *PLoS One* **7**, e42196 (2012).
77. H. Kirst, J. G. García-Cerdán, A. Zurbriggen, A. Melis, Assembly of the light-harvesting chlorophyll antenna in the green alga *Chlamydomonas reinhardtii* requires expression of the TLA2-CpFTSY gene. *Plant Physiol.* **158**, 930–945 (2012).
78. L. Krishnamoorthy *et al*., Copper regulates cyclic-AMP-dependent lipolysis. *Nat. Chem. Biol.* **12**, 586–592 (2016).
79. I. Sizova, M. Fuhrmann, P. Hegemann, A *Streptomyces rimosus* aphVIII gene coding for a new type phosphotransferase provides stable antibiotic resistance to *Chlamydomonas reinhardtii*. *Gene* **277**, 221–229 (2001).
80. N. Depège, S. Bellafiore, J. D. Rochaix, Role of chloroplast protein kinase Stt7 in LHCII phosphorylation and state transition in *Chlamydomonas*. *Science* **299**, 1572–1575 (2003).